TH/P6-14

Integrated particle simulation of neoclassical and turbulence physics in the tokamak pedestal/edge region using XGC[a)]

[1]Chang, C.S., [1]Ku, S., [2]Adams M., [3]D'Azevedo, G., [4]Chen, Y., [5]Cummings, J., [6]Ethier, S., [1]Greengard, L., [6]Hahm, T.S., [7]Hinton, F., [2]Keyes, D., [3]Klasky, S. [6]Lee, W.W. [8]Lin, Z., [8]Nishimura, Y., [4]Parker, S., [6]Samtaney, R., [6]Stotler, D., [1]Weitzner, H., [3]Worley, P., [1]Zorin, D., and the [9]CPES Team

[1]Courant Institute of Mathematical Sciences, New York University, U.S.A.
[2]Columbia University, U.S.A.
[3]Oak Ridge National Laboratory, U.S.A.
[4]University of Colorado, U.S.A.
[5]California Institute of Technology, U.S.A.
[6]Princeton Plasma Physics Laboratory, U.S.A.
[7]University of California at San Diego, U.S.A.
[8]University of California at Irvine, U.S.A.
[9]SciDAC Fusion Simulation Prototype Center for Plasma Edge Simulation

e-mail contact of main author: *cschang@cims.nyu.edu*

Abstract. An integrated gyrokinetic particle simulation with turbulence and neoclassical physics in a diverted tokamak edge plasma has been performed. Neoclassical equilibrium gyrokinetic solutions in the whole edge plasma have been separated from the turbulence activities for the first time, using the massively parallel Jaguar XT3 computer at Oak Ridge National Laboratory. The equilibrium solutions in an H-mode-like edge plasma condition show strongly sheared global ExB and parallel flows in the entire edge plasma including the pedestal and scrape-off regions. In an L-mode-like edge plasma condition, the sheared flows in the pedestal layer are much weaker, supporting the conjecture that the neoclassical flow-shear may play a significant role in the H-mode physics.

The success of ITER is largely dependent upon the achievability of H-mode operation with an edge pedestal of sufficient height [1]. In the edge region, the neoclassical effects can be as important as the turbulence, so that a larg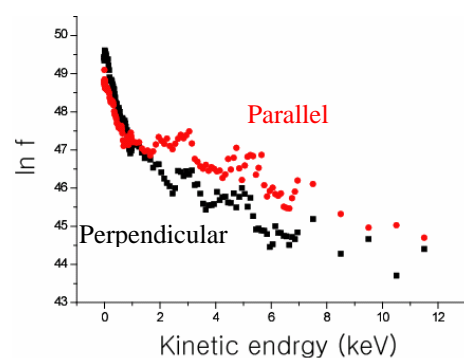e-scale integrated simulation is required to combine the two effects self-consistently. The conventional plasma simulation approach so far has been based upon the phenomenological physics models with a fluid framework. However, the low collisionality of the pedestal plasmas, the ion orbital dynamics in the magnetic X-point geometry [2], the spatially sensitive velocity space boundary [2-5], the orbit squeezing/expansion of the ion banana dynamics from interaction with the self-consistent radial electric field gradients [3,8], the non-Maxwellian nature of the particle distribution function [6,7], the particle source from neutrals, the arbitrary wall shape, and their non-trivial interplay between them are beyond the capability of fluid models (see Fig. 1 for a typical non-Maxwellian ion distribution function in the edge pedestal). A predictive capability requires the development of an edge-specific, large-scale, kinetic code based upon first-principles, which can perform an integrated simulation of the turbulence physics with the neoclassical (and classical) baseline kinetic physics, including the above effects. These features make an edge kinetic simulation much more difficult than a core kinetic simulation.

Fig. 1. Non-Maxwellian ion distribution in an edge pedestal (from XGC-0, 2005 ITPA, TTF)

The previously described full-f edge neoclassical ion particle code XGC-0 [3], which includes all the above baseline neoclassical kinetic physics and solves for ion equilibrium profiles, has been greatly extended to XGC-1 to simulate the integrated neoclassical-turbulence physics self-consistently. The simulation region is from the top of the pedestal to the scrape-off and divertor regions bounded by a material wall. XGC-1 uses a particle-in-cell approach on a massively parallel computing platform. XGC-1 does not study the MHD instabilities, such as ELMs. Instead, it transfers the kinetic bootstrap and pedestal information to an MHD code by a data coupling framework to enable a pedestal-ELM cycle study, which is not a subject of this report. We refer the readers to paper TH/P8-6 at this conference [9].
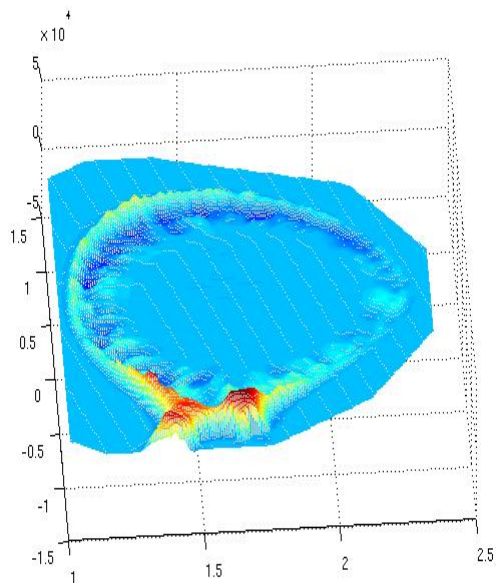

Fig. 2. An early time integrated solution of edge electrostatic potential. Red and blue represent the positive and negative potential, respectively. Sky blue is the zero potential.
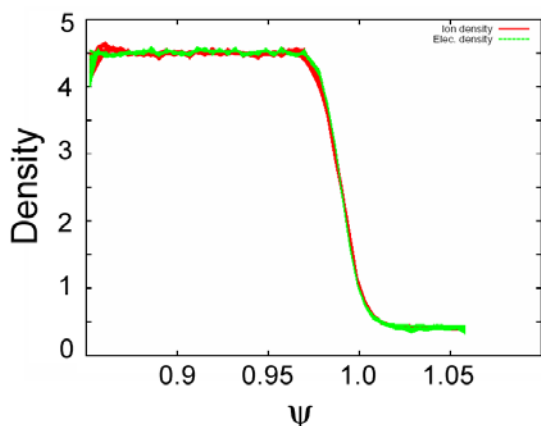

Fig.3. Plasma density $(\times 10^{19} \mathrm{m}^{-3})$ corresponding to Fig.2, normalized to poloidal magnetic flux ψ

The new version XGC-1 includes the full-f electron kinetics, in addition to the full-f ion and neutral dynamics inherited from XGC-0, to perform the turbulence studies together with the baseline kinetic neoclassical phenomena. The large variation of electrostatic potential and plasma on open field lines is included by the full-f ion and electron gyrokinetic dynamics. Both XGCs can also includes the magnetic ripple and neutral beam heating effects. The code will be further developed in the future to include the electromagnetic turbulence physics.

In order to avoid the complications associated with the separatrix geometry, XGC uses the cylindrical coordinate system when evaluating the Lagrangian guiding center particle motions [10]. For solving the Poisson equation, however, the code uses a field-line following coordinate system to take advantage of the fact that plasma purturbations are elongated along magnetic field lines. The usual four-point-averaging technique is used to include the finite gyroradius effects [11]. Neutral particles, from wall-recycling and gas puffing, are simulated concurrently with the plasma particles, providing a self-consistent solution incorporating plasma-material interactions and atomic physics effects. In order to accommodate the X-point geometry and the arbitrary wall geometry, an unstructured triangular mesh is used for the evaluation of the physical observables. The gyrokinetic Poisson equation [12] solves the four-point gyro-averaged charges deposited at the mesh nodes using the PETSc solver library [13].

Figure 2 shows a typical electrostatic potential solution in a poloidal plane at an early time, with integrated neoclassical effects and electrostatic turbulence fluctuations. The pedestal density is $4.5 \times 10^{13} \mathrm{cm}^{-3}$ (see Fig. 3), temperature 1 keV, pedestal width of 1 cm are used. An initial rise

of the potential around the X-point can be observed, arising from the accumulation of positive charges due to the small poloidal component of the magnetic field. The negative potential well (dark blue) is beginning to form just inside the separatrix in the pedestal region, to provide a sheared ExB in the H-mode layer. Positive potential is forming in the scrape-off layer.
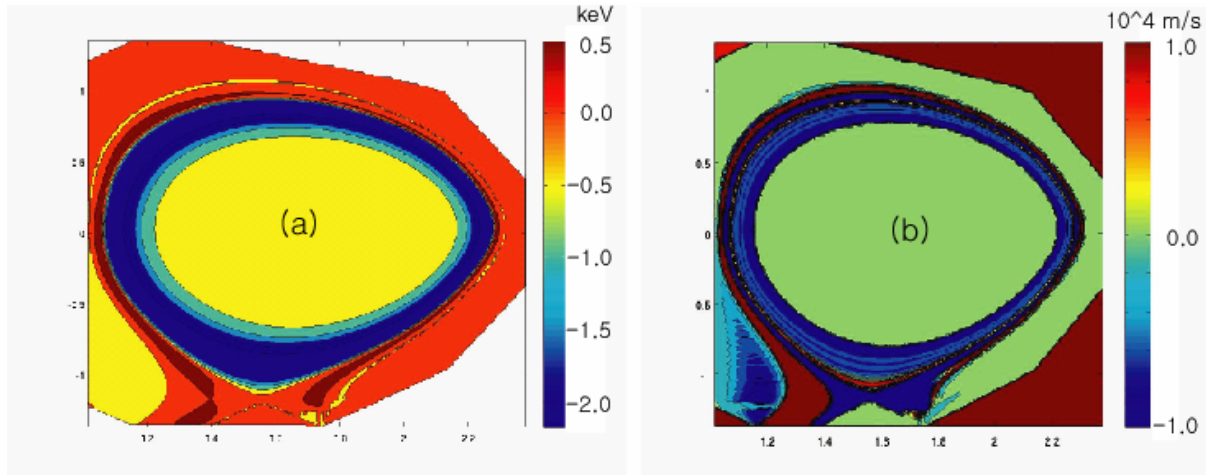

Fig.4. Neoclassical solutions for the electrostatic potential (left) and plasma flow (right) in the edge region of a tokamak plasma.

In Figure 4, the turbulence effects are suppressed by averaging the pential over the turbulent fluctuations to study the baseline neoclassical phenomena in the pedestal and scrape-off plasmas. Such a study has not been possible in the past. The left hand side plot in Fig. 4 gives the electrostatic potential distribution (bright red color represents zero, dark red represents the positive, and the blue hue represents the negative potentials), and the right hand side gives the parallel flow distribution (light green is zero, red hue represents the co-current, and the blue hue represents the counter-current). We can see the formation of negative potential (blue) to -2,000 eV inside the separatrix and positive potential (dark red) to 500 eV in the scrape-off layer. We can also see the formation of the counter-current plasma flow (dark blue) near the separatrix, but co-current flow (brown) in the scrape-off layer. The parallel flow speed shown in the figure is intentionally limited to $|V_{\parallel}| \leq 10^4$ m/s to show more
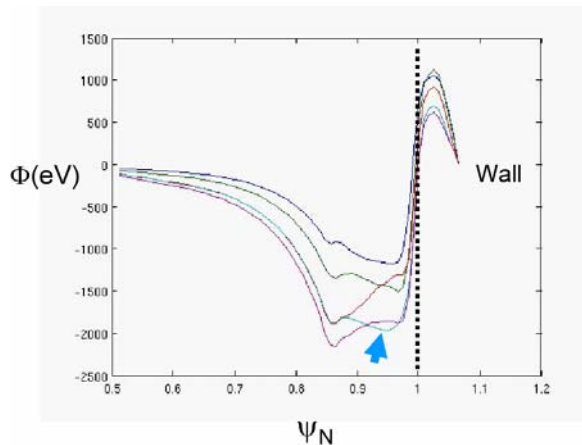

Fig. 5. Development of electrostatic potential profile in the DIII-D edge region. Vertical dotted line shows the separatrix location and the thick blue arrow points to two saturated potential profiles with GAM oscillation.
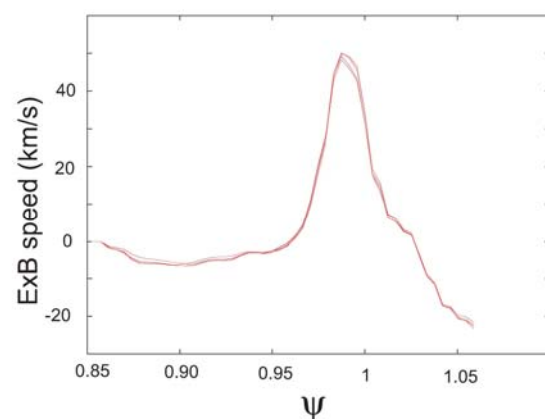
Fig. 6. Strongly sheared ExB poloidal rotation

detailed structures. The local parallel speed can reach near sonic speed well above 10^4 m/s. The electrostatic potential distribution equilibriates in approximately one ion toroidal transit time. However, the parallel flow distribution equilibriates in several ion toroidal transit times. The electron mass in this study is taken to be 1/100 of the deuteron ion, justified by a scanning study in mass ratio.

Figure 5 shows the electrostatic potential ϕ profile corresponding to Fig. 4a, plotted as function of the radial coordinate ψ (poloidal magnetic flux) at the outside midplane. The potential is positive in the scrape-off plasma and negative in the H-mode-like pedestal layer. This potential profile creates a large sheared $E_r \times B$ flow over the entire edge region, as can be seen in Fig. 6, which can have a significant implication to the H-mode transition and sustainment. We examined an L-mode type of pedestal profile and obtained a much weaker ExB shearing rate. The ExB speed is on the order of the poloidal thermal speed. However, a significant fraction of ExB rotation is cancelled by the diagmagnetic flow (se Fig. 7) in the pedestal area, keeping the total poloidal flow speed below Mach 1. The total poloidal flow is shown in red.
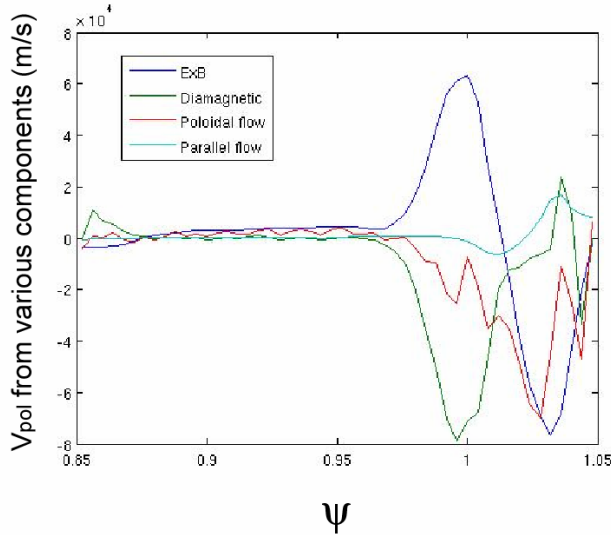

Fig. 7. Various components in poloidal rotation, showing large cancellation between the ExB (blue) and diamagnetic (green) flows in the pedestal.

It is interesting to note that the there is not much diamagnetic flow in the scrape-off layer to cancel the strong ExB flow. Thus, the strong fluid flow there remains in the scrape-off region (red curve).
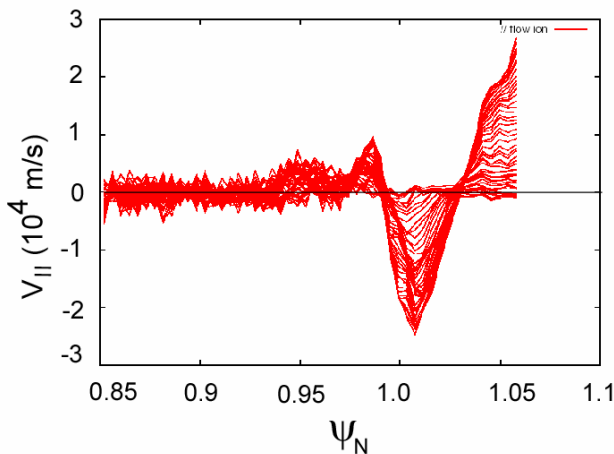

Fig. 8. Sheared parallel rotation in an H-mode-like DIII-D plasma geometry

Figure 8 shows the parallel flow profile time development as function of ψ at the outside midplane. It can be seen that the parallel flow also has significant shear in the entire edge. The parallel flow is negative in the vicinity of the separatrix, then increases to the positive side toward the wall. There is always a positive rotation generation in the pedestal shoulder/top. The region of strong flow shear is somewhat shifted ourward, toward the larger minor radius direction, compared to the ExB flow shear. The poloidal component of equilibrium parallel flow is shown in blue line in Fig. 7 and generally weaker than the poloidal ExB and diamagnetic drifts.

Figure 9 shows another $V_\parallel$ plot with the pedestal width twice the H-mode-like profile shown in Fig. 3. It can be seen that the parallel flow shear is dramatically reduced in the pedestal
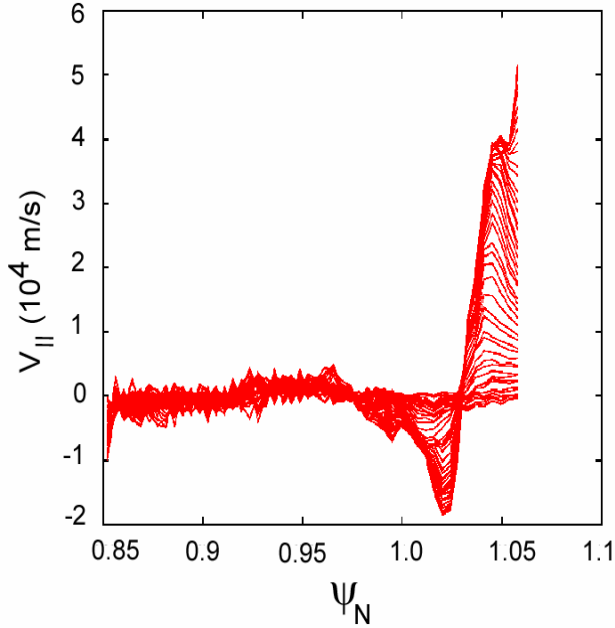
Fig. 9. Parallel velocity profile in a milder pedestal profile. The positive scrape-off flow is more distinctive but the sheared flow in the pedestal layer is significantly
reduced from the H-mode-like pedestal case. Higher neutral recycling rate tends to smooth out the overall flow shear (not shown).

area (notice the difference in the negative vertical scale). On the other hand, the positive flow in the scrape-off layer is dramatically increased to Mach numbers on the order of unity. The specific cases shown here are with negligibly small neutral recycling rate in order to separate the neutral effect from the plasma physics effect. Our previous study with XGC-0 code has shown that the high neutral density in the edge has a tendency to smooth out the velocity shear and to make the parallel velocity monotonically increasing toward the wall. An XGC-0 study result is shown in Fig. 10 (under different edge parameters). It shows how a fixed level of neutral density at an L-mode level ($5 \times 10^{16}\,\mathrm{m}^{-3}$ at the normalized poloidal flux 1.04) smoothes out the parallel flow profile to a monotonically increasing one toward the wall from the pedestal. This probably is what has been observed in L-mode experiments. The thick blue arrow shows the direction of time advancement.

XGC-1 has been verified against a well-known neoclassical parallel rotation formula, valid for a mild-gradient core plasma [14].

$$u_{i\parallel} = (cT_i/eB_p)[k\; \mathrm{d}log T_i/\mathrm{d}r - \mathrm{d}log\; p_i/\mathrm{d}r - (e/T_i)\mathrm{d}\phi/\mathrm{d}r],$$

where k is function of the local ion-ion collision frequency and r is a radial coordinate. Figure 11 shows the numerical solution in blue line and the analytic solution in green line. Black
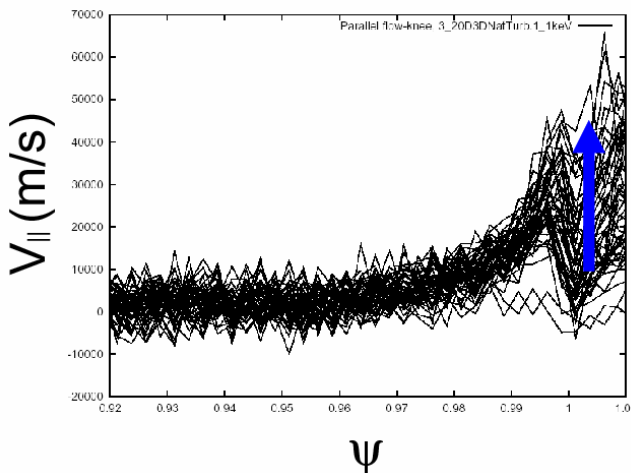

Fig. 10. Neutrals smoothes out the variations in parallel flow profile.

vertical lines show the boundary conditions $\mathrm{d}\phi/\mathrm{d}\psi_r=0$ at $\psi=0.65$ and $\phi=0$ at $\psi=0.85$ in the numerical simulation. It can be seen that the artificial boundary conditions (especially $\phi=0$ at $\psi=0.85$) cause errors near the simulation boundary. Otherwise, the overall agreement is within a few percent. Since the collision frequency dependent k parameter in the above analytic formula is only approximately valid [14], we can only claim an approximate verification. Other mathematical verifications have also been performed with satisfactory results. We note here that the above neoclassical formula is for mild plasma

gradients in the core away from the separatrix and edge effects. We find that the edge plasma rotation does not satisfy this formula at all [7].
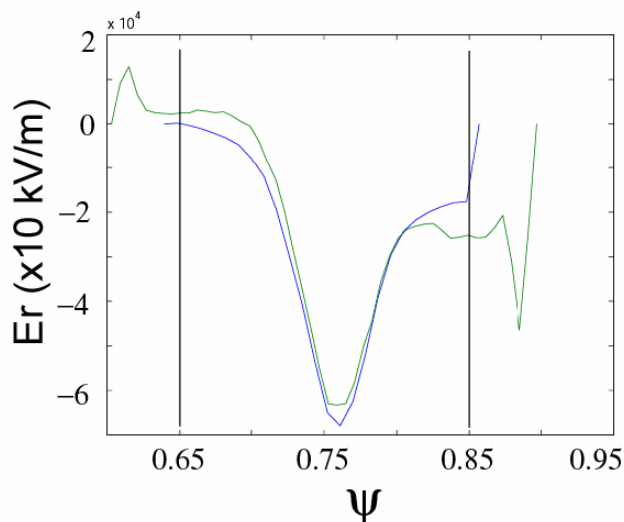

Fig. 11. Verification of the XGC solution (blue line) against the Hinton-Hazeltine's analytic formula (green line). Black vertical lines show the location of the $d\phi/d\psi=0$ at $\psi=0.65$ and $\phi=0$ at $\psi=0.85$ boundary conditions used In the simulation.

The full-f turbulence solutions obtained so far without the averaging process seem to show ringing type of oscillations, coming from the free energy in the imperfect initial particle loading. The averaged neoclassical solution is established long before the ringing type oscillations decayed away. At the present time, we are performing long time simulations to let these ringing type oscillations die out, and to analyze the electrostatic turbulence properties and its effect on plasma transport in the L-mode edge.

The XGC code will be further developed and used to study the L-mode transport, L-H transition, H-mode transport, and pedestal growth, and to couple with an ELM code to study the ELM crash cycle. XGC code will also be coupled with core gyrokinetic codes to provide the boundary conditions needed for core turbulence studies. The toroidal ripple field effect and neutral beam particles are already in XGC. Magnetic error field effect is currently under investigation, in connection with M3D ELM physics. Scrape-off transport and the wall load analysis are other natural inclusions in the XGC study.

References

[1] Groebner R J, Burrell K H, and Seraydarian R P 1990 *Phys. Rev. Lett.* **64** 3015
[2] Chang C S, Ku S, and Weitzner H, *Phys. Plasmas* **9** (2002) 3884; Chang, C.S., Ku, S., et al, IAEA FEC conference, 2004; Phys. Plasmas **11**, 2649 (2004).
[3] Chang C S and Ku S, *Phys. Plasmas* **11** (2004) 2649
[4] Ku, S. H, and Chang, C. S., Phys. Plasmas **11**, (2004) 5626.
[5] Weitzner, H. and Chang, C.S., Phys. Plasmas **11**, (2004) 3060.
[6] Chang, C.S., Ku, S., Contrib. Plasma Phys.46,No.7-9,496–503(2006)
[7] C.S. Chang and the CPES Team, IEA Large Tokamak IA Workshop on Edge Transport in Fusion Plasmas September 11-13, 2006 Kraków, Poland
[8] Hahn, S.H., Ku, S. and Chang, C.S., Phys. Plasmas **12** (2005) 102501.
[9] H. Strauss, L. Sugiyama, C.S. Chang, et al., TH/P-6, 2006 IAEA FEC Conference.
[10] White, R., Phys. Fluid **B2** (1990) 845; Boozer, A.H., Phys. Fluids **27** (1984) 2441; Littlejohn, R. G., Phys. Fluids **28** (1985) 2015.
[11] Lin Z and Lee W W 1995 *Phys. Rev. E* **52** 5646
[12] Lee W W, *Phys. Fluids* **26** (1983) 556
[13] http://www-unix.mcs.anl.gov/petsc/petsc-as/
[14] F.L. Hinton and R.D. Hazeltine, Rev. Mod. Phys. **48** (1976) 239.